# Taming the Antiferromagnetic Beast: Computational Design of Ultrashort Mn–Mn Bonds Stabilized by N-Heterocyclic Carbenes

Marcos A. S. Francisco[+],[a] Felipe Fantuzzi[+],*[b, c, d] Thiago M. Cardozo,[a] Pierre M. Esteves,[a] Bernd Engels,[b] and Ricardo R. Oliveira*[a]

*Dedicated to Professor Marco Antonio Chaer Nascimento on the occasion of his 74th birthday*

**Abstract:** The development of complexes featuring low-valent, multiply bonded metal centers is an exciting field with several potential applications. In this work, we describe the design principles and extensive computational investigation of new organometallic platforms featuring the elusive manganese-manganese bond stabilized by experimentally realized N-heterocyclic carbenes (NHCs). By using DFT computations benchmarked against multireference calculations, as well as MO- and VB-based bonding analyses, we could disentangle the various electronic and structural effects contributing to the thermodynamic and kinetic stability, as well as the experimental feasibility, of the systems. In particular, we explored the nature of the metal-carbene interaction and the role of the ancillary $\eta^6$ coordination to the generation of $Mn_2$ systems featuring ultrashort metal-metal bonds, closed-shell singlet multiplicities, and positive adiabatic singlet-triplet gaps. Our analysis identifies two distinct classes of viable synthetic targets, whose electrostructural properties are thoroughly investigated.

## Introduction

The pioneering work on rhenium clusters by Cotton in the 1960s, with the attribution of the first double,[1] triple,[2] and quadruple[3] bonds between transition metal atoms, has opened

[a] M. A. S. Francisco,[+] Prof. Dr. T. M. Cardozo, Prof. Dr. P. M. Esteves, Prof. Dr. R. R. Oliveira
Instituto de Química
Universidade Federal do Rio de Janeiro
Av. Athos da Silveira Ramos 149
21941909 Rio de Janeiro (Brazil)
E-mail: rrodrigues.iq@gmail.com

[b] Dr. F. Fantuzzi,[+] Prof. Dr. B. Engels
Institut für Physikalische und Theoretische Chemie
Julius-Maximilians-Universität Würzburg
Emil-Fischer-Straße 42, 97074 Würzburg (Germany)
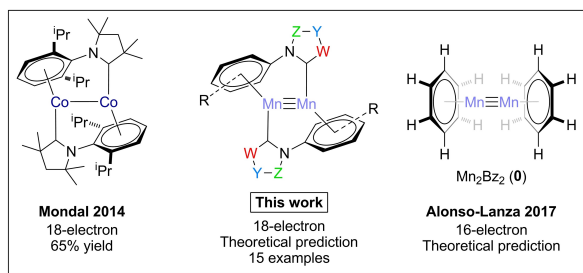E-mail: felipe.fantuzzi@uni-wuerzburg.de

[c] Dr. F. Fantuzzi[+]
Institut für Anorganische Chemie
Julius-Maximilians-Universität Würzburg
Am Hubland, 97074 Würzburg (Germany)

[d] Dr. F. Fantuzzi[+]
Institute for Sustainable Chemistry & Catalysis with Boron
Julius-Maximilians-Universität Würzburg
Am Hubland, 97074 Würzburg (Germany)

[+] These authors contributed equally to this work.

📱 Supporting information for this article is available on the WWW under https://doi.org/10.1002/chem.202101116

the intriguing field of multiple metal-metal bonding.[4] Since then, this topic has expanded significantly,[5] with a myriad of novel compounds featuring homonuclear or heteronuclear metal-metal bonds,[6] and some whose bond orders between the metal atoms are even greater than four.[7] The motivation for studying these systems arises from fundamentals[8] to a desire of elucidating novel molecular motifs with peculiar electronic structures and bonding properties, which culminates in potential chemical applications. As a consequence, compounds featuring metal-metal bonds are now widely used in organometallic catalysis,[9] small molecule activation,[10] photochemistry,[11] and in the development of metal-organic frameworks[12] and extended metal atom chains.[13] Metal-metal bonds also play a crucial role in biological processes, not only stabilizing low-valence states and initiating oxidative addition reactions in metalloenzymes,[14] but also allowing the transfer of phosphate groups in for example DNA polymerases.[15]

In striking difference with other homonuclear diatomic molecules featuring first-row transition metals, the naked $Mn_2$ species is a weakly bonded van der Waals dimer featuring antiferromagnetic coupling and a very long metal-metal distance of 3.7–3.9 Å.[16] Up to now, only a few systems featuring Mn–Mn bonds in the range of 2.2–2.7 Å are known.[17] Recently, Alonso-Lanza and co-workers[18] predicted that an ultrashort Mn–Mn bond of about 1.8 Å can be achieved in the 16-electron $Mn_2Bz_2$ complex (Bz=$C_6H_6$, Scheme 1). However, the benzene ligand is not sufficiently bulky to stabilize the metal centers in $Mn_2Bz_2$ and prevent them from further decomposition due to undesired reactions. In order to circumvent this problem and to design experimentally stable organometallic platforms featuring

**Chemistry–A European Journal**

Full Paper
doi.org/10.1002/chem.202101116

**Chemistry Europe**
European Chemical
Societies Publishing

**Scheme 1.** Selected systems featuring ligand-stabilized metal-metal bonds.

reactive metal-metal bonds, it is necessary to use appropriate ligands which are capable of shielding the metal centers.
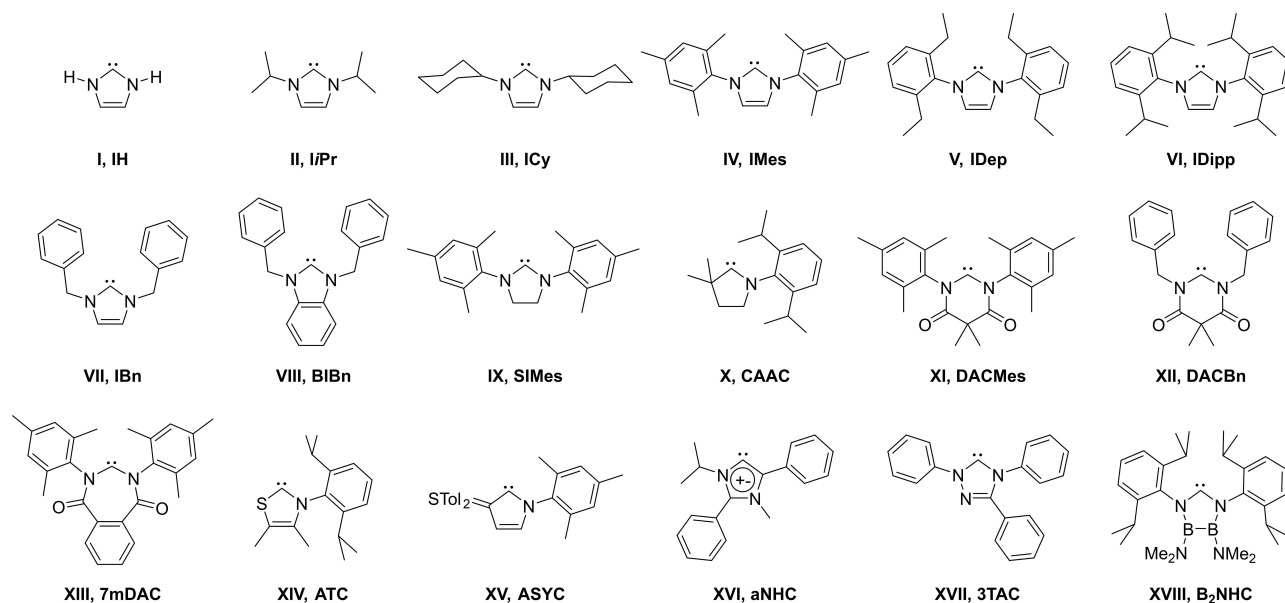
Since the first synthesis of a persistent N-heterocyclic carbene (NHC) by Arduengo et al.,[19] there is an increasing interest in the coordination chemistry of these compounds. The diversity of structures and electronic properties of NHCs and their complexes encouraged intense research in distinct topics,[20] from fundamentals to for example catalysis,[21] medicinal,[22] and photochemical[23] applications. Indeed, NHCs have been instrumental in enhancing the photophysical properties of organometallic compounds of first-row, Earth-abundant transition metal elements,[24] particularly those of iron[25] and cobalt,[26] making them promising materials for light-harvesting and photocatalysis. Another remarkable property of NHCs is their ability to stabilize unusual and reactive main group[27] and transition metal species. Consequently, completely new structures have been isolated and characterized, such as the boron dimer featuring double and triple bonds,[28] molecular silicon oxides,[29] doubly bonded $Si_2$,[30] $Ge_2$,[31] $Sn_2$,[32] $Al_2$,[33] and $Ga_2$,[34] phosphorus clusters,[35] low-valent Be,[36] B,[37] C,[38] and Al[39] species, coinage metal atoms,[40] and many others. Moreover,

NHCs have also been systematically incorporated in periodic systems[41] and extended networks,[42] and their ability to stabilize main group dimers into these structures is currently under investigation.[43]

In parallel with the extraordinary development of the coordination chemistry of NHCs with main group and mono-nuclear transition metal species, these ligands have also been used to prepare stable derivatives of low-valent metal compounds featuring metal-metal bonds. Indeed, complexes of dinuclear $Fe^0$ stabilized by IMes and IDipp were synthesized, with Fe-Fe distances of 2.621 and 2.583 Å.[44] Stable low-valent, dinuclear metal-metal systems were also obtained by coordination with cyclic (alkyl)(amino) carbenes (CAAC),[45] particularly for homonuclear Au[46] and Co[47] motifs. In both cases, the metal−metal bond distances are in the range of 2.5–2.7 Å, and the systems have closed-shell singlet ground states. For $Co_2(CAAC)_2$, an ancillary $\eta^6$ coordination of the Dipp substituents at the nitrogen CAAC to the cobalt atoms is also present (Scheme 1), allowing the metal centers to achieve an 18-electron configuration.

Inspired by the vast body of literature illustrating the ability of NHCs to stabilize elusive main group and transition metal species, in this work we perform a thorough computational exploration of the use of these ligands for stabilizing the manganese dimer (Scheme 1). In our approach, we investigate distinct $Mn_2L_2$ species following the design principles depicted in Scheme 1, and make use of DFT calculations benchmarked against a multireference approach to investigate their main electrostructural features, aiming at selecting potential targets for future experimental realization.

A complete list of the carbene ligands explored herein is shown in Scheme 2. They are numbered by Roman numerals, while Arabic numerals refer to their corresponding $Mn_2$ complexes. Ligands **I–VII** possess the imidazol-2-ylidene core



**Scheme 2.** Carbene ligands investigated herein.

**Chemistry–A European Journal**

Full Paper
doi.org/10.1002/chem.202101116

**Chemistry Europe**
European Chemical
Societies Publishing

with distinct substituents at the nitrogen atoms, namely hydrogen (**I, IH**), isopropyl (**II, I$i$Pr**), cyclohexane (**III, ICy**), mesityl (**IV, IMes**), diethylphenyl (**V, IDep**), diisopropylphenyl (**VI, IDipp**), and benzyl (**VII, IBn**). Ligand **VIII** is the benzyl derivative of benzoimidazolylidene (**BIBn**),[48] while **IX** and **X** are the mesityl-substituted saturated imidazol-2-ylidene (**SIMes**) and the cyclic (alkyl)(amino) carbene (**CAAC**).[45] Ligands **XI–XIII** are diamidocarbenes, the first two having a six-membered core with Mes (**DACMes**)[49] and Bn (**DACBn**) substituents, while the latter is a Mes-substituted seven-membered ring carbene (**7mDAC**).[50] The remaining ligands are the amino(thio)carbene (**XIV, ATC**),[51] amino (sulfur-ylide) carbene (**XV, ASYC**),[52] the abnormal NHC (**XVI, aNHC**),[53] triazolecarbene (**XVII, 3TAC**), and the diboron NHC (**XVIII, B$_2$NHC**).[54]

## Computational Details

We start our investigation by analyzing the Mn$_2$Bz$_2$ system. This molecule was chosen for a preliminary benchmark study (see the Supporting Information for details) in order to derive an appropriate functional for the DFT calculations of the NHC-stabilized compounds, and also as a model system to investigate the role of the $\eta^6$ coordination on the stability of the Mn$_2$ dimer. By comparing the DFT results with high-level calculations based on the complete active space self-consistent field (CASSCF) method,[55] with active spaces of up to 14 electrons and 14 orbitals, and additional N-electron valence state second-order perturbation theory (NEVPT2)[56] calculations, we adopted the PBE[57]-D3[58](BJ)[59]/def2-SVP;def2-TZVP (Mn)[60] level of theory as it provided the best results in comparison with the multireference calculations (from now on this basis set will be referred as bs1). Additionally, for a better comparison with the results obtained by Alonso-Lanza and others,[18] we also performed spin-polarized DFT calculations with plane-wave basis sets. These results are discussed in the Supporting Information.

In all cases, geometry optimizations and hessian calculations were obtained at the mentioned DFT level considering closed-shell singlet wave functions. All optimized geometries were characterized as minimum energy structures as all vibrational frequencies have positive eigenvalues. Additional calculations were performed considering triplet multiplicities in order to obtain the vertical and adiabatic singlet-triplet gaps ($\Delta_{ST}$). Unless otherwise stated, the $\Delta_{ST}$ values refer to the vertical ones. The following notation is used:

$$\Delta_{ST} = E_{triplet} - E_{singlet} \qquad (1)$$

In order to gain insights into the bonding situation of the systems, we performed calculations based on the intrinsic bond orbital (IBO),[61] natural bond orbital (NBO),[62] natural resonance theory (NRT),[63] and generalized valence bond at the perfect-pairing approximation (GVB-PP)[64] methods, the latter with the 6-31G* basis set. These distinct approaches gave qualitatively similar descriptions. We will mainly focus on the results obtained by analysis of the canonical Kohn-Sham molecular orbitals (MOs) and the GVB-PP mono-occupied orbitals, while further calculations obtained with the other approaches are found in the Supporting Information. Mayer bond orders (MBOs)[65] were also estimated for all systems.

Finally, we calculated the dissociation enthalpies at 298.15 K ($DH^0_{298.15}$) and the thermochemistry of the ligand exchange reaction from Mn$_2$Bz$_2$ to Mn$_2$L$_2$ aiming at investigating the stabilization gain provided by the distinct carbene moieties. The kinetic stability of

$\eta^6$-coordinated Mn$_2$L$_2$ systems was also investigated. The enthalpy of ligand exchange, $\Delta H_{ex}$, is calculated as:

$$\Delta H_{ex} = H_{Mn_2L_2} + 2\,H_{Bz} - H_{Mn_2Bz_2} - 2\,H_L \qquad (2)$$

where $H$ includes the zero-point energy and all thermal contributions to enthalpy, and L varies from L = **I, IH** to L = **XVIII, B$_2$NHC** (Scheme 2). For this discussion, we also included truncated, uncoupled model systems of the type Mn$_2$(Bz)$_2$(IH)$_2$ (**mod-A** and **mod-B**). The stability of these species is analyzed by calculating the binding enthalpy, $\Delta H_b$ defined as:

$$\Delta H_b = H_{Mn_2(Bz)_2(IH)_2} - H_{Mn_2Bz_2} - 2\,H_{IH} \qquad (3)$$

All DFT calculations with Gaussian basis sets were performed in Gaussian 16,[66] while those with plane waves were done in VASP.[67] The multireference calculations were performed using ORCA 4.2.[68] The MBOs were obtained with Multiwfn 3.7.[69] NBO and NRT calculations were done with the NBO 7.0 program,[70] while the GVB-PP computations were performed with VB2000.[71]

## Results and Discussion

### Computational description of Mn$_2$Bz$_2$ and the $\eta^6$ coordination

In this section, we discuss the electronic structure of Mn$_2$Bz$_2$, as it provides a basis for understanding the $\eta^6$ interaction between manganese and the phenyl group in the carbene-stabilized Mn$_2$ systems. At the CASSCF(14,14)/bs1 level of theory, the Mn$_2$Bz$_2$ species converges to a structure of $D_{6h}$ symmetry, with an Mn–Mn bond of 1.74 Å (Table S1 in the Supporting Information). This metal-metal bond is slightly shortened in comparison to the one reported by Alonso-Lanza and co-workers[18] using DFT with plane-wave basis set. The weight of the closed-shell configuration is 0.62, with no particular excited configuration contributing more than 0.025 to the overall CASSCF wave function. The biradical character index $y_0$ of Mn$_2$Bz$_2$, calculated following the Yamaguchi formula[72] as shown in Equations (S1)–(S4), is 0.03 at this level of theory. Indeed, the exploratory DFT calculations using either the spin-polarized formalism with plane waves (Table S2) or the broken-symmetry approach also converged to a closed-shell singlet with no spin density at the metal atoms. At the NEVPT2/CASSCF(10,10)/bs1 level, the vertical $\Delta_{ST}$ gap is 35.9 kcal mol$^{-1}$, with dynamic correlation stabilizing the triplet by 13.5 kcal mol$^{-1}$. Taken together, these results give strong evidence that the singlet state has no biradical character, and that the system can be appropriately described by single-reference methods.

As for the DFT calculations with a singlet closed-shell wave function and Gaussian basis sets, our results indicate that hybrid functionals significantly underestimate both the Mn–Mn bond distance and $\Delta_{ST}$ in comparison to those obtained with multireference approaches, as shown in Table S3. The best agreement with the CASSCF/NEVPT2 results comes from calculations in the PBE–D3(BJ)/bs1 level, where the Mn–Mn bond length is 1.73 Å, and $\Delta_{ST}$ is 30.6 kcal mol$^{-1}$. At this level of theory, the optimized structure also has $D_{6h}$ symmetry, with the Mn$_2$ moiety pointing to the center of the benzene rings. The angle between

**Chemistry–A European Journal**

Full Paper
doi.org/10.1002/chem.202101116

**Chemistry Europe**
European Chemical
Societies Publishing

the centroid of the benzene ring and the two Mn atoms, herein labeled as $\theta$(Bz–Mn–Mn), is, therefore, 180° (Figure 1a). Interestingly, an isoenergetic, staggered isomer with a slightly distorted $D_{6d}$ symmetry is also found (Figure S2), suggesting that the benzene ligands in $Mn_2Bz_2$ have some degree of fluxionality, and that the system could be described as a nanowheel-type compound.

In order to investigate the bonding situation in $Mn_2Bz_2$, we show in Figure 1b the canonical Kohn-Sham molecular orbitals of the system. HOMO-3 is formed by the $+,+$ combination, with $a_{1g}$ symmetry, of the Mn $d_{z^2}$ orbitals along the intermetallic vector, and composes the metal-metal sigma bond. In turn, HOMO-2 and HOMO-1 are degenerate sets of two orbitals, related to the Mn–Mn $\pi$ and $\delta$ bonds. These five orbitals, which are bonding with respect to the Mn–Mn bond, are contrasted with the remaining degenerate, low-lying HOMOs, which present antibonding character in the intermetallic region. The formal bond order of 3, as suggested by bonding/antibonding

orbital counting, is corroborated by distinct computational approaches. The calculated Mayer Bond Order of the Mn–Mn bond is 2.45, while that calculated using the NRT approach is exactly 3.00. Inspection of the GVB-PP orbitals, depicted in Figure 1c, reveals three bonding pairs located at the metal –metal region, related to the formation of one sigma and two $\pi$ bonds, with the remaining metal d orbitals participating explicitly in the metal-benzene bonding. A similar bonding profile is obtained by inspecting the intrinsic bond orbitals (IBOs), whose metal-metal and metal-benzene bonding pairs are shown in Figure S3.

In opposition to their antibonding profile with respect to the Mn–Mn bond, the degenerate HOMOs present a strong bonding character in the Mn–Bz region. The influence of these orbitals on the metal-ligand interaction is also evidenced by analyzing the structure of the system where the electrons occupying these orbitals are removed, thus leading to the $[Mn_2Bz_2]^{4+}$ tetracation (Figure 1a). In this case, the molecular
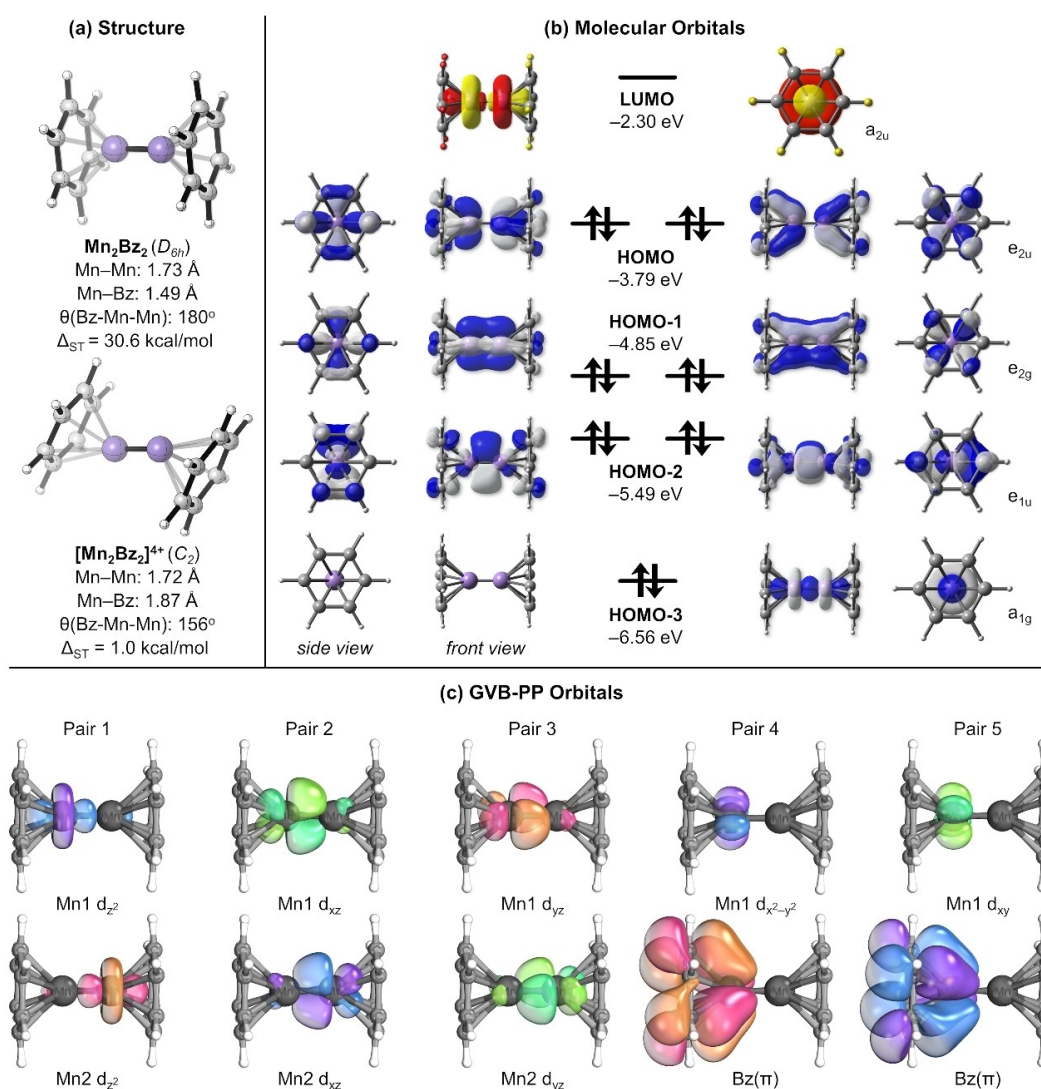


**Figure 1.** a) Structure and selected properties $Mn_2Bz_2$ and $[Mn_2Bz_2]^{4+}$ at their optimized geometries. b) Canonical Kohn-Sham molecular orbitals of $Mn_2Bz_2$. c) Selected GVB-PP orbitals of $Mn_2Bz_2$. The DFT calculations were performed at the PBE–D3(BJ)/bs1 level of theory (see text for details).

**Chemistry–A European Journal**

Full Paper
doi.org/10.1002/chem.202101116

**Chemistry Europe**
European Chemical
Societies Publishing

symmetry is reduced to $C_2$, and $\theta$(Bz–Mn–Mn) goes to 156°. The Mn–Bz bond distance elongates by about 0.4 Å (or 25%), reaching 1.84 Å in the tetracation. This leads to a severe stability loss in the multiply charged system. A reduction of almost 30 kcal mol$^{-1}$ in $\Delta_{ST}$ is experienced by the system after removal of the $e_{2u}$ electrons, thus highlighting the important role of the $\eta^6$ interaction in the stabilization of the manganese dimer in its closed-shell singlet state. Interestingly, the Mn–Mn bond length is not disturbed in the [Mn$_2$Bz$_2$]$^{4+}$ system, despite the formal bond order increase to a value of five. This can be attributed to the Coulomb repulsion of the positive charges, which prevents the equilibrium bond length between the two MnBz fragments to be shortened.

Finally, the LUMO of Mn$_2$Bz$_2$ (Figure 1b) has an $a_{2u}$ symmetry, and is composed of a +,– combination of the two Mn d$_{z^2}$ orbitals. It is, therefore, antibonding with respect to the Mn–Mn bond. The HOMO-LUMO gap is 1.49 eV at the PBE–D3(BJ)/bs1 level of theory, more than twofold as that calculated for the tetracation (0.61 eV). Interestingly, interaction with this orbital will play a role in the bonding situation of the Mn$_2$L$_2$ systems, as we discuss in the following sections.

## Overview of the Mn$_2$L$_2$ systems

Table 1 characterizes the various Mn$_2$ complexes with the ligands depicted in Scheme 2. The optimized structures of selected complexes are given in Figure 2 (other structures can be found in Figure S4). Inspection of the structures clearly indicates that in all cases the Mn$_2$ moiety is shielded by the carbene ligands. To investigate the influence of the covalent connection between benzene and the carbene moiety, we also calculated two model systems of type **Mn$_2$(Bz)$_2$(IH)$_2$**, where the carbene and the benzene ligands are not covalently connected. These two isomers, whose geometries are fully optimized minimum energy structures of the potential energy hypersurface of **Mn$_2$(Bz)$_2$(IH)$_2$**, are shown in Figure 3, and are labeled herein as **mod-A** and **mod-B**. While the **mod-A** structure, where the NHC moieties are terminal ligands oriented parallel with respect to the Mn–Mn bond, resembles the ones observed in most of the Mn$_2$L$_2$ systems, in **mod-B** the NHCs are bridging ligands oriented perpendicularly across the Mn–Mn bond. To our surprise, **mod-B** is more stable than **mod-A**. Consequently, Mn$_2$ systems composed of more flexible carbenes exhibit structural features which are more closely related to **mod-B**.

Besides various geometrical parameters, Table 1 also contains the computed vertical and adiabatic singlet-triplet gaps [$\Delta_{ST}$, Eq. (1)], the dissociation enthalpies ($DE^0_{298.15}$), and the ligand exchange enthalpies [$\Delta H_{ex}$, Eq. (2)] of all the Mn$_2$ species studied herein, together with the binding enthalpies [$\Delta H_b$, Eq. (3)] of the truncated systems **mod-A** and **mod-B**. Table 1 underlines that the combination of the benzene and carbene moieties indeed leads to considerably more stable complexes than the parent system Mn$_2$Bz$_2$, as expected based on the 18-electron rule. The positive $\Delta H_{ex}$ values of ligands without benzene moieties (**I–III**) show that the $\eta^6$ coordination is more important for the stabilization than the carbene moieties. The Mn–Mn bond lengths of these complexes (**1–3**), which are in the range of 1.73–1.75 Å, are shorter than those of the carbene complexes featuring $\eta^6$ coordination (1.87–2.08 Å), but still

**Table 1.** Selected structural, electronic, and thermochemical properties of the various Mn$_2$L$_2$ systems studied herein, obtained at the PBE–D3(BJ)/bs1 level of theory.

| Species | Ligand | $r$(Mn–Mn) [Å] | MBO | $r$(Bz–Mn) [Å] | $r$(C–Mn) [Å] | $\theta$(Bz–Mn–Mn) [°] | $\Delta_{ST}$[a] [kcal mol$^{-1}$] | $\Delta H_{ex}$ [kcal mol$^{-1}$] | $DH^0_{298.15}$ [kcal mol$^{-1}$] |
|---|---|---|---|---|---|---|---|---|---|
| Mn$_2$Bz$_2$ | Bz | 1.73 | 2.45 | 1.49 | – | 180 | +30.6 (+24.1) | – | +85.6 |
| **mod-A** | Bz; IH | 1.98 | 1.92 | 1.66 | 2.00 | 146 | +28.5 (+12.3) | −87.2[b] | +172.8 |
| **mod-B** | Bz; IH | 2.17 | 1.06 | 1.56 | 2.05 | 169 | +11.8 (+8.1) | −99.6[b] | +185.3 |
| **1** | IH | 1.74 | 3.86 | – | 1.92 | – | −2.8 (+8.5) | +29.1 | +56.5 |
| **1b** | IH | 1.96 | 2.61 | – | 1.95 | – | −4.8 (–) | +57.9 | +27.7 |
| **2** | IiPr | 1.75 | 3.68 | – | 1.93 | – | −3.1 (−9.0) | +27.2 | +58.5 |
| **3** | ICy | 1.75 | 3.65 | – | 1.92 | – | −3.7 (−9.7) | +22.5 | +63.4 |
| **4** | IMes | 1.88 | 2.42 | 1.94 | 2.00 | 140 | +15.7 (+7.2) | −66.4 | +152.0 |
| **5** | IDep | 1.90 | 2.32 | 1.93 | 2.03 | 144 | +17.3 (+1.8) | −74.9 | +160.5 |
| **6** | IDipp | 1.87 | 2.45 | 1.92 | 2.02 | 143 | +17.9 (+8.1) | −77.1 | +162.8 |
| **7** | IBn | 2.08 | 1.40 | 1.57 | 1.99[c] | 150 | +18.6 (+11.6) | −88.0 | +173.6 |
| **8** | BIBn | 2.07 | 1.34 | 1.57 | 1.98[c] | 151 | +16.2 (+7.2) | −93.6 | +179.2 |
| **9** | SIMes | 2.12 | 1.70 | 1.62 | 1.96 | 129 | +8.7 (+4.2) | −75.9 | +161.6 |
| **10** | CAAC | 1.86 | 2.36 | 1.94 | 1.96 | 141 | +21.2 (+9.4) | −79.1 | +164.7 |
| **11** | DACMes | 2.19 | 1.24 | 1.62 | 1.90 | 115 | +15.7 (+6.1) | −101.2 | +186.8 |
| **11′**[d] | DACMes | 2.13 | 1.22 | 1.60 | 1.87 | 119 | +20.3 (+13.9) | −100.7 | +186.3 |
| **12** | DACBz | 2.08 | 1.45 | 1.58 | 1.985[c] | 150 | +11.0 (−2.9) | −94.1 | +179.7 |
| **12′**[d] | DACBz | 2.02 | 1.36 | 1.58 | 2.041[c] | 159 | +17.2 (+3.7) | −110.7 | +196.3 |
| **13** | 7mDAC | 2.25 | 1.04 | 1.62 | 1.90 | 109 | +13.3 (+3.9) | −93.0 | +178.7 |
| **14** | ATC | 1.97 | 2.00 | 1.62 | 2.00 | 149 | +18.7 (+3.9) | −90.4 | +176.0 |
| **15** | ASYC | 1.86 | 2.48 | 1.93[e] | 2.015[e] | 142[e] | +8.6 (+3.2) | −78.4 | +164.0 |
| **16** | aNHC | 1.85 | 2.56 | 2.28[e] | 2.010[e] | 137[e] | +2.7 (−2.3) | −48.6 | +134.2 |
| **17** | 3TAC | 2.05 | 1.90 | 1.61 | 1.99 | 139 | +10.7 (−2.7) | −55.4 | +141.0 |
| **18** | B2NHC | 1.91 | 2.22 | 1.92 | 1.97 | 131 | +14.9 (–) | −86.0 | +171.6 |

[73]
[a] Values in parentheses are the adiabatic $\Delta_{ST}$ gaps. [b] For **mod-A** and **mod-B**, $\Delta H_{ex}$ is equivalent to the binding enthalpy, $\Delta H_b$. [c] Smallest value. [d] The non-coordinating substituent at nitrogen is replaced by hydrogen. [e] Average value.

**Chemistry–A European Journal**

Full Paper
doi.org/10.1002/chem.202101116

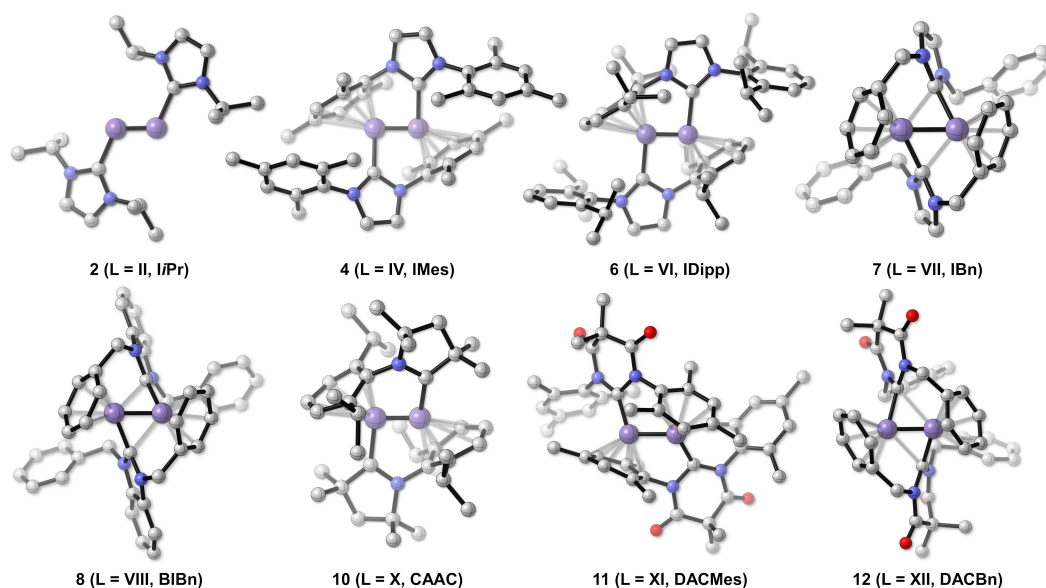**Chemistry Europe**
European Chemical
Societies Publishing

**Figure 2.** 3D pictures of selected $Mn_2L_2$ species at their optimized structures at the PBE–D3(BJ)/bs1 level, evidencing the distinct bonding motifs adopted by the systems as a consequence of the complex interplay between electronic and steric effects.
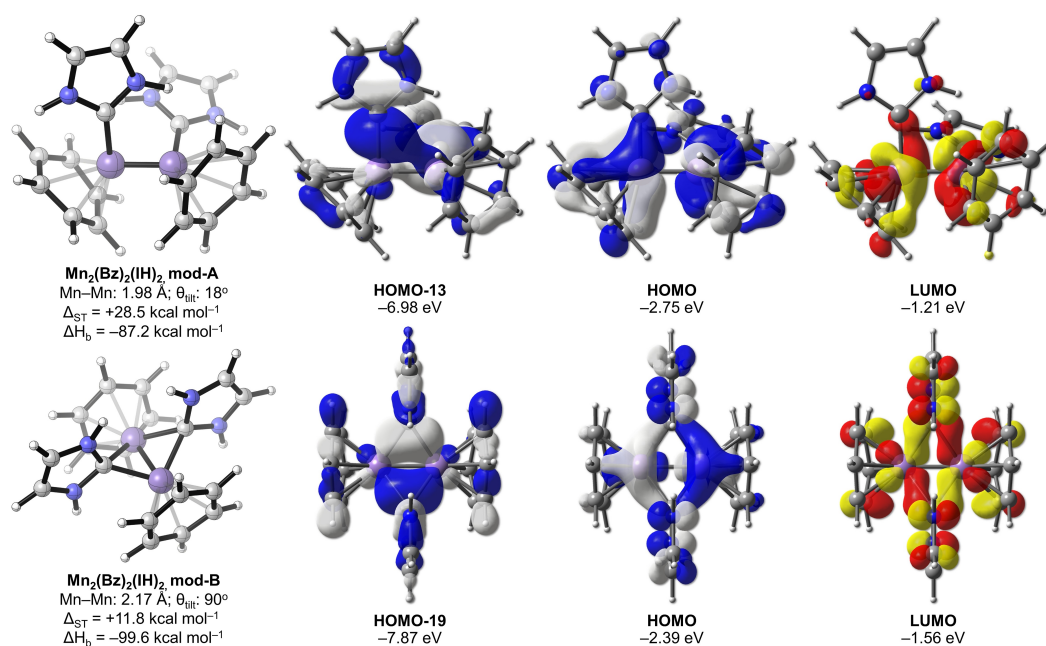


**Figure 3.** Structure, properties, and selected canonical Kohn-Sham molecular orbitals of the $Mn_2(Bz)_2(IH)_2$ model systems **mod-A** (top) and **mod-B** (bottom).

slightly longer than that of the parent $Mn_2Bz_2$ compound. The $\Delta H_{ex}$ values of ligands in which the aromatic rings are directly coupled to the nitrogen of the imidazol-2-ylidene carbene (ligands **IV–VI**) range between −66 and −77 kcal mol$^{-1}$. If the flexibility is increased by the presence of $CH_2$ bridges (ligands **VII–VIII**), the $\Delta H_{ex}$ values increase to −88 and −94 kcal mol$^{-1}$, revealing that the stability of the complexes is narrowed if the carbene and the phenyl moieties cannot adopt their optimal positions. This is underlined by the binding enthalpy of −99 kcal mol$^{-1}$ computed for the model system $Mn_2(Bz)_2(IH)_2$

**mod-B** in which both ligands can orient independently. Accordingly, all $DH^0_{298.15}$ values of the $Mn_2L_2$ complexes featuring the $\eta^6$ coordination (**4**–**18**) are significantly larger than that of $Mn_2Bz_2$, highlighting once more the thermodynamic stability of these systems.

Figure 3 indicates that in the optimal geometry (**mod-B**) the benzene moieties behave as terminal ligands with $\eta^6$ orientation, while the NHCs are interacting with $Mn_2$ as bridging ligands, forming a butterfly-shaped $C_2Mn_2$ structure. In **mod-B** the carbene moieties stand perpendicular to the Mn–Mn bond,

**Chemistry–A European Journal**

**Full Paper**
doi.org/10.1002/chem.202101116

**Chemistry Europe**
European Chemical
Societies Publishing

while they are parallelly oriented in all of the $Mn_2L_2$ systems where the aromatic ring is directly attached to the carbene backbone. This orientation is necessary so that the $\eta^6$ coordination can be formed in such molecules featuring rigid carbene ligands. As a consequence, the carbene moieties are also shifted from the middle of the $Mn_2$ bond to the Mn centers, and the systems adopt a structure similar to **mod-A**. The decrease in stabilization experienced by these systems in comparison to the optimal geometry of **mod-B** can be analyzed by comparing the energies of the model systems. The difference in $\Delta H_b$ going from **mod-B** to **mod-A** is about 12 kcal mol$^{-1}$, and results from the reorientation of carbene moieties and the deviation of the benzene moiety from the perfect $\eta^6$ coordination. The importance of both effects is underlined by analyzing the structures of the $Mn_2$ complexes (**7** and **8**) with ligands **VII** and **VIII**. In both cases, the higher flexibility is not solely used to enforce a perfect $\eta^6$ orientation. In contrast, the system adopts a compromise between the optimal orientations of the carbene and the benzene moieties. Interestingly, in the highly stable complexes (e.g., **mod-B**, **7**, and **8**) with (partly) perpendicularly oriented NHCs, the $Mn_2$ bond is considerably longer ($>2.07$ Å) than in those complexes in which the carbenes adopt parallel orientations ($<1.9$ Å).

For the various complexes featuring imidazol-2-ylidene carbenes, strongly stabilized systems are obtained if the flexibility of the ligand is high enough to allow a good compromise between the perfect positions of the carbenes and the aromatic rings. By comparing these complexes with the ones featuring other carbene backbones, it becomes obvious that the nature of the carbene also influences the stability of the systems. Inspection of the $\Delta H_{ex}$ values reveals that the most stable complex among the ones featuring the ligands shown in Scheme 2 is the one bearing the **DACMes** ligand (**11**, L=**XI**, $\Delta H_{ex}=-101$ kcal mol$^{-1}$). This can be attributed to the fact that the diamidocarbene ligands have the greatest π-accepting character among the ones studied herein, as also evidenced by the relatively short C–Mn bond of **11** and **13**. Conversely, replacement of imidazol-2-ylidene by **CAAC** (**10**, L=**X**) does not lead to a significant change in $\Delta H_{ex}$, even with the latter presenting the largest $\Delta_{ST}$ gap among the systems of Scheme 2. Compounds with sulfur (**14**, L=**IV**, **ATC**) or boron (**18**, L=**XVIII**, **B$_2$NHC**) in the carbene backbone also behave very similar to those of the classic NHC ligands, indicating that similar bonding effects are present. As these species are more difficult to handle experimentally and we do not predict exceptionally high stabilities, they will not be further discussed.

Interestingly, complexes **11** and **13** have large $\Delta H_{ex}$ values despite being the systems where the $\theta$(Bz–Mn–Mn) angles deviate the most from the ones of the perfect Bz–Mn orientation. It is therefore obvious that the flexibility of these ligands is not high enough (Figure 2), and could be increased if CH$_2$ groups are introduced in the substituents at the nitrogen. However, the replacement of the Mes groups in **11** by the Bn groups in **12** does not make the $\Delta H_{ex}$ of the latter more negative, in spite of its higher flexibility. This happens because of a steric clash between the Bn groups that are not involved in the $\eta^6$ coordination, which destabilizes **12** despite its better

Mn–L interaction. This becomes obvious after analyzing the $\Delta H_{ex}$ values of the model systems **11'** and **12'** (Figure S5), where these nonparticipating groups are replaced by hydrogen. This modification makes **12'** the system where $\Delta H_{ex}$ has the most negative value among all the ones studied herein ($-111$ kcal mol$^{-1}$), being around 10 kcal mol$^{-1}$ larger than that of **11'**. This result evidences once more the important role of the $\eta^6$ coordination for the stabilization of the Mn–Mn bond, and that the complex interplay between the nature and flexibility of the carbene, the relative position of the interacting phenyl rings, and steric effects of nonparticipating substituents must be taken into account for designing complexes capable of stabilizing highly reactive species featuring metal-metal bonds.

We also investigated the kinetic stability of the $Mn_2L_2$ complexes featuring the $\eta^6$ coordination. These calculations were conducted for the phenyl-substituted imidazolylidene (**IPh**) ligand, and the results are summarized in Figure 4 (see Figures S7 and S8 for selected relaxed scans). The free energy of dissociation of the Mn–C bond of **Mn$_2$(IPh)$_2$** (**A**) to compound **B** is uphill by 31.2 kcal mol$^{-1}$. In turn, ligand dissociation from **B** is also uphill by 43.2 kcal mol$^{-1}$, with compound **C** lying 74.4 kcal mol$^{-1}$ above **A**. The dissociation of the second Mn–C bond, which leads to compound **D**, has a kinetic barrier (**TS1**) of 40.1 kcal mol$^{-1}$, with **D** lying 110.5 kcal mol$^{-1}$ above **A**. In this structure, the $Mn_2$ motif is only interacting with the phenyl moiety. Ligand dissociation from **D** to form isolated $Mn_2$ and 2 IPh species is nearly equiergic. The coupling of the two IPh ligands to form the alkene **PhI=IPh** is exergonic by merely 6.4 kcal mol$^{-1}$. Therefore, our results strongly suggest that the $\eta^6$-coordinated $Mn_2L_2$ complexes are kinetically stable towards dissociation to isolated $Mn_2$ and carbene ligands, and that their formation from the isolated constituents should not be kinetically hindered.

Comparing the stability of the various complexes, the following questions arise: i) Why do the NHC moieties try to
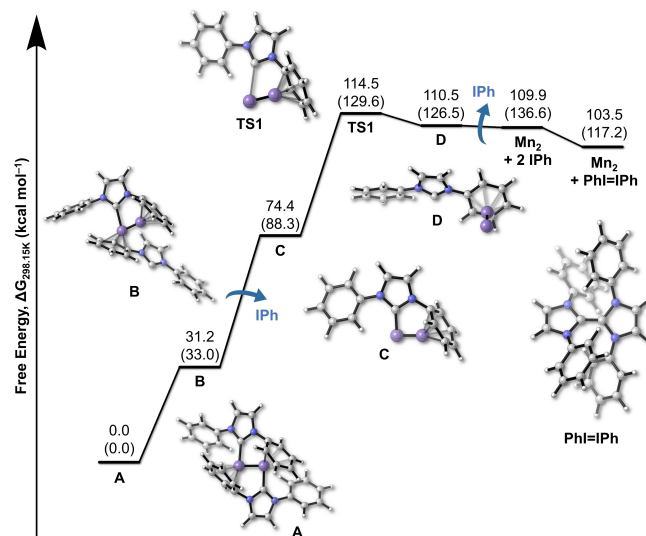


**Figure 4.** Relative Gibbs free energy [kcal mol$^{-1}$] profile of the dissociation of **Mn$_2$(IPh)$_2$** (**A**) into $Mn_2$ + 2 IPh at the PBE–D3(BJ)/def2SVP level of theory. The relative ZPE-corrected electronic energies are shown in parentheses.

orient perpendicular to the $Mn_2$ bond in the systems featuring $\eta^6$ coordination, following **mod-B**, and ii) why does it lead to a lengthening of the $Mn_2$ bond? iii) How does the bonding situation change going from perpendicularly oriented carbenes positioned across the Mn–Mn bond to parallelly oriented carbenes which are shifted towards the Mn centers? iv) Why does the $C_2Mn_2$ ring is butterfly-shaped rather than planar? These issues are addressed in the following section.

### Understanding the electrostructural properties of $Mn_2L_2$

In order to investigate the origin of the main structural and electronic features of the $Mn_2L_2$ systems, we focus on the description of the model systems **mod-A** and **mod-B** (Figure 3), as well as on the corresponding systems **1** and **1 b** (see Figure 5), which features the **IH** ligand, but not the benzene rings. Selected structural properties and canonical Kohn–Sham molecular orbitals of **mod-A** and **mod-B** are shown in Figure 3. A comparison of the structures of **1** and **1 b** can be visualized in Figure 5. The molecular orbitals of **1** are shown in Figure 6.

The isomer **mod-A**, which bears structural similarities with most of the $Mn_2L_2$ systems, is characterized by the presence of terminal NHC and Bz ligands at both metal centers, with the NHCs parallelly oriented to the metal-metal bond. Due to the steric hindrance between the N–H hydrogen and the hydrogen attached to benzene, the two NHCs are positioned almost orthogonal to each other. Because of the parallel orientation of the NHCs, the benzene rings distort significantly from their optimal position due to sterics, and $\theta$(Bz–Mn–Mn) reaches 146° for **mod-A**. In contrast, if the NHCs are perpendicularly oriented across the Mn–Mn bond, such as in **mod-B**, the benzene rings can accommodate in a more appropriate position, keeping $\theta$(Bz–Mn–Mn) as close to 180° as possible and shortening the metal–benzene distance. As the $\eta^6$ coordination contributes the most for the stabilization of the systems studied herein, **mod-B** is approximately 12 kcal mol$^{-1}$ more stable than **mod-A**. Additionally, the surrounding benzene ligands decrease electron density in the intermetallic region with respect to that of the $Mn_2$ dimer in the absence of $\eta^6$ coordination. This effect also
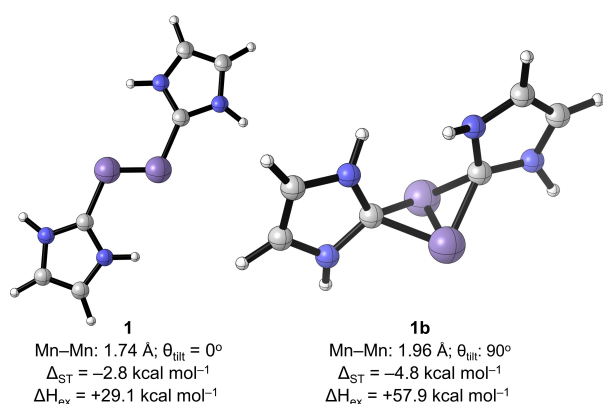


LUMO
−1.74 eV

HOMO
−2.05 eV

HOMO-1
−2.35 eV

HOMO-2
−3.20 eV

HOMO-3
−3.36 eV

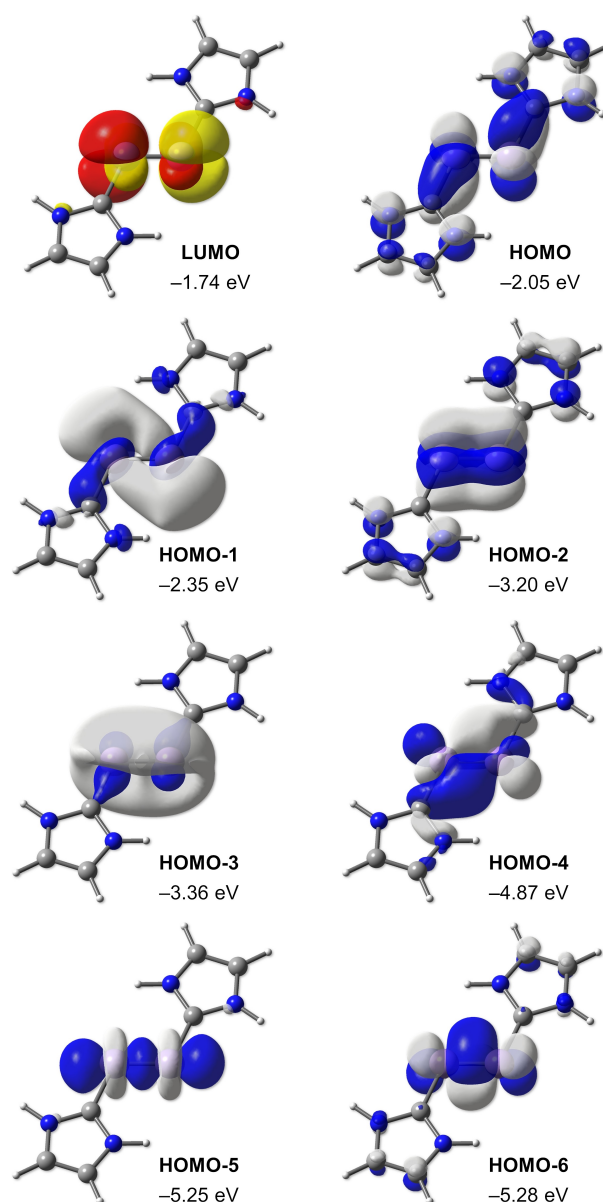HOMO-4
−4.87 eV

HOMO-5
−5.25 eV

HOMO-6
−5.28 eV

**Figure 6.** Canonical Kohn-Sham molecular orbitals of **1** at the PBE–D3(BJ)/bs1 level of theory.

plays a major role, and explains the destabilizing nature of **1 b** (Figure 5). The preferred orientation of the NHCs is, therefore, dictated by the $\eta^6$ coordination, whose interaction is more effective if the carbenes occupy bridging positions, while at the same time enabling this orientation due to depletion of intermetallic electron density.

The preference of the $\eta^6$ coordination over the carbene-metal bond in driving the optimal geometries of the compounds studied herein is also visualized by inspection of the bonding situation of the distinct model systems. These can be assessed by analyzing their corresponding canonical molecular orbitals, as shown in Figure 3, and the ones of the isolated $Mn_2Bz_2$ and $(NHC)_2$ fragments in the same geometries as those of the model compounds. The distortion from the



**1**
Mn–Mn: 1.74 Å; $\theta_{tilt}$ = 0°
$\Delta_{ST}$ = −2.8 kcal mol$^{-1}$
$\Delta H_{ex}$ = +29.1 kcal mol$^{-1}$

**1b**
Mn–Mn: 1.96 Å; $\theta_{tilt}$: 90°
$\Delta_{ST}$ = −4.8 kcal mol$^{-1}$
$\Delta H_{ex}$ = +57.9 kcal mol$^{-1}$

**Figure 5.** Structure and selected properties of **1** and **1 b** at the PBE–D3(BJ)/bs1 level of theory.

**Chemistry–A European Journal**

Full Paper
doi.org/10.1002/chem.202101116

**Chemistry
Europe**
European Chemical
Societies Publishing

$\theta(Bz-Mn-Mn) = 180°$ in both model systems removes the degeneracies observed in the orbitals of the optimized $Mn_2Bz_2$ (see Figure 1 to visualize the optimal orbitals). The sigma donation of the carbenes to $Mn_2Bz_2$ in **mod-A** is illustrated for example in HOMO-13. In turn, the HOMO of **mod-A** involves interaction of the HOMO of $Mn_2Bz_2$ with the empty p orbitals of the NHCs. This evidences that π back donation is indeed at play in the metal–NHC interaction. In contrast, the HOMO of **mod-B** is formed by the interaction of the LUMO of $Mn_2Bz_2$ and the vacant p orbitals of the NHCs. This occupied orbital is strongly antibonding with respect to the Mn–Mn bond, as it is composed of the $+,-$ combination of the Mn $d_{z^2}$ atomic orbitals. This picture is in accordance with the metal-metal bond lengthening of **mod-B** in comparison to those of **mod-A** and the optimized $Mn_2Bz_2$. Furthermore, inspection of the energies of **1** and **1 b** (Figure 5) clearly shows that the metal-NHC interaction when the ligands occupy bridging positions is less favored than the one featuring terminal NHCs, which is particularly true for the case where no $\eta^6$ interaction takes place. This also explains the smaller HOMO-LUMO gap and $\Delta_{ST}$ of **mod-B** in comparison to those of **mod-A**. The greater thermodynamic stability of **mod-B**, therefore, can be attributed preferentially to the better orientation of the $\eta^6$ coordination, and not due to the position of the NHCs.

When the carbene ligands are perpendicularly oriented across the Mn–Mn bond, a butterfly-shaped $C_2Mn_2$ moiety is formed. This bonding motif can be rationalized in terms of the carbene interaction with the π orbitals of $Mn_2$. In this sense, the planar structure is avoided so that the carbenes do not interact with the same metal-metal π orbital. If the carbenes are completely orthogonal, they would interact with distinct metal-metal π systems. However, bringing the carbenes to this orientation is not favored due to steric repulsion of the nitrogen substituents, which also contributes to the high energy of **1 b** in comparison to **1** (Figure 5). The $C_2Mn_2$ butterfly structure, therefore, is obtained as the result of an interplay between electronic effects driven by the carbenes and steric effects driven by the substituent groups at the nitrogen.

One last question remains to be addressed. In our $Mn_2L_2$ systems, the ones where no $\eta^6$ coordination is formed are those featuring the smallest metal-metal bond lengths. This is discussed by the analysis of the canonical molecular orbitals of **1**, which are shown in Figure 6. HOMO-6, HOMO-5, and HOMO-4 are related to the σ and π bonds of $Mn_2$, while HOMO-3 and HOMO-2 compose the δ bonds, with HOMO-3 also including contribution from the Mn 4 s orbitals. HOMO-1 is a nonbonding orbital, whose lobes are pointing to the vacant sites of the *trans*-bent structure. Finally, HOMO is π antibonding with respect to the $Mn_2$ dimer, and π bonding with respect to the carbene moieties, suggesting the presence of metal-to-ligand π-backbonding interactions. In contrast to the $Mn_2L_2$ systems featuring $\eta^6$ coordination, a formal bond order of 4 is therefore expected to $Mn_2$ in **1–3**, which is supported by the Mayer bond order values (3.65 to 3.86) and also by NRT and GVB-PP calculations (see Section S2.2). This higher bond order explains why the Mn–Mn bond in **1–3** is shorter than those of the other $Mn_2L_2$ systems. However, the absence of $\eta^6$ coordination severely affects the stability of the systems, as evidenced by their negative $\Delta_{ST}$ values (Table 1) and the narrow HOMO–LUMO gap of **1**, which is merely 0.31 eV.

Given the remarkable similarity between the structures obtained herein and those synthesized for complexes featuring $Co_2$ and $Fe_2$ (Figure S6), it becomes relevant to investigate if our findings can be extrapolated to other transition metal complexes featuring NHC-stabilized metal-metal bonds. Such calculations are currently underway, and the results will be presented in due course.

## Conclusion

In summary, we have reported herein the first examples of 18-electron organometallic platforms featuring low-valent, ultrashort manganese–manganese bonds stabilized by experimentally realized N-heterocyclic carbene ligands. Our thorough computational exploration indicates the synthetic feasibility of these systems and identifies their main electrostructural features. In particular, our analysis reveals which factors contribute the most to generating stable, closed-shell singlet structures with positive adiabatic singlet-triplet gaps, and how they affect the metal-metal bond. The ancillary $\eta^6$ coordination from the phenyl substituent of the carbene backbone is a fundamental requirement for the formation of kinetically and thermodynamically stable $Mn_2L_2$ complexes. If this interaction is present, two classes of potential synthetic targets emerge, depending on the ligand flexibility. For rigid carbenes, structures where these ligands occupy terminal positions are obtained, with Mn–Mn bond lengths ranging from 1.8–2.0 Å. On the other hand, systems featuring bridging carbenes are formed if more flexible substituents are involved. The latter structures are thermodynamically favored, even with the drawback of increasing the metal-metal bond length to values in the range of 2.0–2.2 Å. By disentangling electronic and steric effects, we could identify that the preference of systems featuring bridging carbenes over those where these ligands occupy terminal positions is due to a better orientation of the $\eta^6$ coordination, which also contributes to the bridging coordination by depleting intermetallic electron density. From our analysis, we suggest that **IDipp** (L=**VI**), **IBn** (L=**VII**), **BIBn** (L=**VIII**), **CAAC** (L=**X**), and **DACMes** (L=**XI**) are the best candidates as ligands for the experimental realization of $Mn_2L_2$ systems. These results clearly show that new and exciting avenues in Lewis base chemistry with metal-metal bonding are yet to be explored.

## Conflict of Interest

The authors declare no conflict of interest.

[1] J. A. Bertrand, F. A. Cotton, W. A. Dollase, *J. Am. Chem. Soc.* **1963**, *85*, 1349–1350.

[2] a) M. J. Bennett, F. A. Cotton, R. A. Walton, *J. Am. Chem. Soc.* **1966**, *88*, 3866–3867; b) M. J. Bennett, F. A. Cotton, R. A. Walton, *Proc. R. Soc. London Ser. A* **1968**, *303*, 175–192.

[3] a) F. A. Cotton, N. F. Curtis, C. B. Harris, B. F. G. Johnson, S. J. Lippard, J. T. Mague, W. R. Robinson, J. S. Wood, *Science* **1964**, *145*, 1305–1307; b) F. A. Cotton, *Inorg. Chem.* **1965**, *4*, 334–336; c) F. A. Cotton, C. B. Harris, *Inorg. Chem.* **1965**, *4*, 330–333.

[4] F. A. Cotton, *Acc. Chem. Res.* **1978**, *11*, 225–232.

[5] J. F. Berry, C. C. Lu, *Inorg. Chem.* **2017**, *56*, 7577–7581.

[6] C.-S. Cao, Y. Shi, H. Xu, B. Zhao, *Coord. Chem. Rev.* **2018**, *365*, 122–144.

[7] a) J. P. Collman, R. Boulatov, *Angew. Chem. Int. Ed.* **2002**, *41*, 3948–3961; *Angew. Chem.* **2002**, *114*, 4120–4134; b) T. Nguyen, A. D. Sutton, M. Brynda, J. C. Fettinger, G. J. Long, P. P. Power, *Science* **2005**, *310*, 844–847; c) Y.-C. Tsai, C.-W. Hsu, J.-S. K. Yu, G.-H. Lee, Y. Wang, T.-S. Kuo, *Angew. Chem. Int. Ed.* **2008**, *47*, 7250–7253; *Angew. Chem.* **2008**, *120*, 7360–7363; d) Y.-L. Huang, D.-Y. Lu, H.-C. Yu, J.-S. K. Yu, C.-W. Hsu, T.-S. Kuo, G.-H. Lee, Y. Wang, Y.-C. Tsai, *Angew. Chem. Int. Ed.* **2012**, *51*, 7781–7785; *Angew. Chem.* **2012**, *124*, 7901–7905; e) L. J. Clouston, R. B. Siedschlag, P. A. Rudd, N. Planas, S. Hu, A. D. Miller, L. Gagliardi, C. C. Lu, *J. Am. Chem. Soc.* **2013**, *135*, 13142–13148; f) N. V. S. Harisomayajula, A. K. Nair, Y.-C. Tsai, *Chem. Commun.* **2014**, *50*, 3391–3412.

[8] a) J. Joy, D. Danovich, M. Kaupp, S. Shaik, *J. Am. Chem. Soc.* **2020**, *142*, 12277–12287; b) E. Levi, D. Aurbach, C. Gatti, *Molecules* **2021**, *26*, 304.

[9] a) I. G. Powers, C. Uyeda, *ACS Catal.* **2017**, *7*, 936–958; b) C. M. Farley, C. Uyeda, *Trends Chem.* **2019**, *1*, 497–509.

[10] a) F. Akagi, T. Matsuo, H. Kawaguchi, *Angew. Chem. Int. Ed.* **2007**, *46*, 8778–8781; *Angew. Chem.* **2007**, *119*, 8934–8937; b) C. M. Thomas, *Comments Inorg. Chem.* **2011**, *32*, 14–38; c) Y. Lee, F. T. Sloane, G. Blondin, K. A. Abboud, R. García-Serres, L. J. Murray, *Angew. Chem. Int. Ed.* **2015**, *54*, 1499–1503; *Angew. Chem.* **2015**, *127*, 1519–1523; d) K. M. Gramigna, D. A. Dickie, B. M. Foxman, C. M. Thomas, *ACS Catal.* **2019**, *9*, 3153–3164; e) F. Fantuzzi, M. A. C. Nascimento, B. Ginovska, R. M. Bullock, S. Raugei, *Dalton Trans.* **2021**, *50*, 840–849.

[11] a) T. J. Meyer, J. V. Caspar, *Chem. Rev.* **1985**, *85*, 187–218; b) A. F. Heyduk, D. G. Nocera, *Science* **2001**, *293*, 1639–1641; c) A. R. Corcos, J. S. Pap, T. Yang, J. F. Berry, *J. Am. Chem. Soc.* **2016**, *138*, 10032–10040; d) A. Das, J. H. Reibenspies, Y.-S. Chen, D. C. Powers, *J. Am. Chem. Soc.* **2017**, *139*, 2912–2915; e) T. J. Whittemore, C. Xue, J. Huang, J. C. Gallucci, C. Turro, *Nat. Chem.* **2020**, *12*, 180–185.

[12] H.-C. Hu, H.-S. Hu, B. Zhao, P. Cui, P. Cheng, J. Li, *Angew. Chem. Int. Ed.* **2015**, *54*, 11681–11685; *Angew. Chem.* **2015**, *127*, 11847–11851.

[13] a) S.-A. Hua, M.-C. Cheng, C.-h. Chen, S.-M. Peng, *Eur. J. Inorg. Chem.* **2015**, *2015*, 2510–2523; b) J. A. Chipman, J. F. Berry, *Chem. Rev.* **2020**, *120*, 2409–2447.

[14] P. A. Lindahl, *J. Inorg. Biochem.* **2012**, *106*, 172–178.

[15] L. Perera, W. A. Beard, L. G. Pedersen, S. H. Wilson, *Inorg. Chem.* **2017**, *56*, 313–320.

[16] a) C. J. Barden, J. C. Rienstra-Kiracofe, H. F. Schaefer, *J. Chem. Phys.* **2000**, *113*, 690–700; b) S. Yamamoto, H. Tatewaki, H. Moriyama, H. Nakano, *J. Chem. Phys.* **2006**, *124*, 124302; c) C. Angeli, A. Cavallini, R. Cimiraglia, *J. Chem. Phys.* **2008**, *128*, 244317.

[17] a) I. Bernal, J. D. Korp, W. A. Herrmann, R. Serrano, *Chem. Ber.* **1984**, *117*, 434–444; b) J. Chai, H. Zhu, A. C. Stückl, H. W. Roesky, J. Magull, A. Bencini, A. Caneschi, D. Gatteschi, *J. Am. Chem. Soc.* **2005**, *127*, 9201–9206; c) A. E. Ashley, R. T. Cooper, G. G. Wildgoose, J. C. Green, D. O'Hare, *J. Am. Chem. Soc.* **2008**, *130*, 15662–15677; d) L. Fohlmeister, S. Liu, C. Schulten, B. Moubaraki, A. Stasch, J. D. Cashion, K. S. Murray, L. Gagliardi, C. Jones, *Angew. Chem. Int. Ed.* **2012**, *51*, 8294–8298; *Angew. Chem.* **2012**, *124*, 8419–8423.

[18] T. Alonso-Lanza, J. W. González, F. Aguilera-Granja, A. Ayuela, *J. Phys. Chem. C* **2017**, *121*, 25554–25560.

[19] A. J. Arduengo, R. L. Harlow, M. Kline, *J. Am. Chem. Soc.* **1991**, *113*, 361–363.

[20] M. N. Hopkinson, C. Richter, M. Schedler, F. Glorius, *Nature* **2014**, *510*, 485–496.

[21] a) *N-Heterocyclic Carbenes in Transition Metal Catalysis, Vol. 21*, (Ed.: F. Glorius), Springer Berlin Heidelberg, **2007**; b) N. Marion, S. Díez-González, S. P. Nolan, *Angew. Chem. Int. Ed.* **2007**, *46*, 2988–3000; *Angew. Chem.* **2007**, *119*, 3046–3058; c) S. Díez-González, N. Marion, S. P. Nolan, *Chem. Rev.* **2009**, *109*, 3612–3676; d) U. S. D. Paul, U. Radius, *Eur. J. Inorg. Chem.* **2017**, *2017*, 3362–3375.

[22] a) K. M. Hindi, M. J. Panzner, C. A. Tessier, C. L. Cannon, W. J. Youngs, *Chem. Rev.* **2009**, *109*, 3859–3884; b) W. Liu, R. Gust, *Coord. Chem. Rev.* **2016**, *329*, 191–213; c) N. Wiratpruk, A. Noor, C. A. McLean, P. S. Donnelly, P. J. Barnard, *Dalton Trans.* **2020**, *49*, 4559–4569.

[23] a) L. Mercs, M. Albrecht, *Chem. Soc. Rev.* **2010**, *39*, 1903; b) M. Elie, J.-L. Renaud, S. Gaillard, *Polyhedron* **2018**, *140*, 158–168; c) S. Urinda, G. Das, A. Pramanik, P. Sarkar, *J. Phys. Chem. C* **2019**, *123*, 14216–14222; d) N. U. D. Reshi, J. K. Bera, *Coord. Chem. Rev.* **2020**, *422*, 213334; e) A. Mavroskoufis, M. Jakob, M. N. Hopkinson, *ChemPhotoChem* **2020**, *4*, 5147–5153.

[24] O. S. Wenger, *J. Am. Chem. Soc.* **2018**, *140*, 13522–13533.

[25] a) T. Duchanois, T. Etienne, M. Beley, X. Assfeld, E. A. Perpète, A. Monari, P. C. Gros, *Eur. J. Inorg. Chem.* **2014**, *2014*, 3747–3753; b) T. Duchanois, T. Etienne, C. Cebrián, L. Liu, A. Monari, M. Beley, X. Assfeld, S. Haacke, P. C. Gros, *Eur. J. Inorg. Chem.* **2015**, *2015*, 2469–2477; c) L. Liu, T. Duchanois, T. Etienne, A. Monari, M. Beley, X. Assfeld, S. Haacke, P. C. Gros, *Phys. Chem. Chem. Phys.* **2016**, *18*, 12550–12556; d) P. Chábera, K. S. Kjaer, O. Prakash, A. Honarfar, Y. Liu, L. A. Fredin, T. C. B. Harlang, S. Lidin, J. Uhlig, V. Sundström, R. Lomoth, P. Persson, K. Wärnmark, *J. Phys. Chem. Lett.* **2018**, *9*, 459–463; e) T. Duchanois, L. Liu, M. Pastore, A. Monari, C. Cebrián, Y. Trolez, M. Darari, K. Magra, A. Francés-Monerris, E. Domenichini, M. Beley, X. Assfeld, S. Haacke, P. Gros, *Inorganics* **2018**, *6*, 63; f) O. S. Wenger, *Chem. Eur. J.* **2019**, *25*, 6043–6052; g) L. Lindh, P. Chábera, N. W. Rosemann, J. Uhlig, K. Wärnmark, A. Yartsev, V. Sundström, P. Persson, *Catalysts* **2020**, *10*, 315; h) N. W. Rosemann, P. Chábera, O. Prakash, S. Kaufhold, K. Wärnmark, A. Yartsev, P. Persson, *J. Am. Chem. Soc.* **2020**, *142*, 8565–8569; i) H. Tatsuno, K. S. Kjær, K. Kunnus, T. C. B. Harlang, C. Timm, M. Guo, P. Chábera, L. A. Fredin, R. W. Hartsock, M. E. Reinhard, S. Koroidov, L. Li, A. A. Cordones, O. Gordivska, O. Prakash, Y. Liu, M. G. Laursen, E. Biasin, F. B. Hansen, P. Vester, M. Christensen, K. Haldrup, Z. Németh, D. Sárosiné Szemes, É. Bajnóczi, G. Vankó, T. B. Van Driel, R. Alonso-Mori, J. M. Glownia, S. Nelson, M. Sikorski, H. T. Lemke, D. Sokaras, S. E. Canton, A. O. Dohn, K. B. Møller, M. M. Nielsen, K. J. Gaffney, K. Wärnmark, V. Sundström, P. Persson, J. Uhlig, *Angew. Chem. Int. Ed.* **2020**, *59*, 364–372; *Angew. Chem.* **2020**, *132*, 372–380.

[26] a) S. Kaufhold, N. W. Rosemann, P. Chábera, L. Lindh, I. Bolaño Losada, J. Uhlig, T. Pascher, D. Strand, K. Wärnmark, A. Yartsev, P. Persson, *J. Am. Chem. Soc.* **2021**, *143*, 1307–1312; b) K. Yatsuzuka, K. Yamauchi, K. Kawano, H. Ozawa, K. Sakai, *Sustain. Energy Fuels* **2021**, *5*, 740–749.

[27] a) V. Nesterov, D. Reiter, P. Bag, P. Frisch, R. Holzner, A. Porzelt, S. Inoue, *Chem. Rev.* **2018**, *118*, 9678–9842; b) E. Welz, J. Böhnke, R. D. Dewhurst, H. Braunschweig, B. Engels, *J. Am. Chem. Soc.* **2018**, *140*, 12580–12591; c) S. Kundu, S. Sinhababu, V. Chandrasekhar, H. W. Roesky, *Chem. Sci.* **2019**, *10*, 4727–4741; d) P. Schmid, F. Fantuzzi, J. Klopf, N. B. Schröder, R. D. Dewhurst, H. Braunschweig, V. Engel, B. Engels, *Chem. Eur. J.* **2021**, *27*, 5160–5170; e) T. Brückner, F. Fantuzzi, T. E. Stennett, I. Krummenacher, R. D. Dewhurst, B. Engels, H. Braunschweig, *Angew. Chem. Int. Ed.* **2021**, *60*, 13661–13665; *Angew. Chem.* **2021**, *133*, 13774–13779; f) S. Hagspiel, F. Fantuzzi, R. D. Dewhurst, A. Gärtner, F. Lindl, A. Lamprecht, H. Braunschweig, *Angew. Chem. Int. Ed.* **2021**, *60*, 13666–13670; *Angew. Chem.* **2021**, *133*, 13780–13784.

[28] a) Y. Wang, B. Quillian, P. Wei, C. S. Wannere, Y. Xie, R. B. King, H. F. Schaefer, P. v. R. Schleyer, G. H. Robinson, *J. Am. Chem. Soc.* **2007**, *129*, 12412–12413; b) H. Braunschweig, R. D. Dewhurst, K. Hammond, J. Mies,

Chemistry–A European Journal

Full Paper
doi.org/10.1002/chem.202101116

Chemistry
Europe
European Chemical
Societies Publishing

K. Radacki, A. Vargas, *Science* **2012**, *336*, 1420–1422; c) H. Braunschweig, R. D. Dewhurst, *Angew. Chem. Int. Ed.* **2013**, *52*, 3574–3583; *Angew. Chem.* **2013**, *125*, 3658–3667; d) J. Böhnke, H. Braunschweig, W. C. Ewing, C. Hörl, T. Kramer, I. Krummenacher, J. Mies, A. Vargas, *Angew. Chem. Int. Ed.* **2014**, *53*, 9082–9085; *Angew. Chem.* **2014**, *126*, 9228–9231; e) H. Braunschweig, R. D. Dewhurst, *Organometallics* **2014**, *33*, 6271 6277.

[29] Y. Wang, M. Chen, Y. Xie, P. Wei, H. F. Schaefer, P. v. R. Schleyer, G. H. Robinson, *Nat. Chem.* **2015**, *7*, 509–513.

[30] Y. Wang, Y. Xie, P. Wei, R. B. King, H. F. Schaefer, P. von R. Schleyer, G. H. Robinson, *Science* **2008**, *321*, 1069–1071.

[31] A. Sidiropoulos, C. Jones, A. Stasch, S. Klein, G. Frenking, *Angew. Chem. Int. Ed.* **2009**, *48*, 9701–9704; *Angew. Chem.* **2009**, *121*, 9881–9884.

[32] C. Jones, A. Sidiropoulos, N. Holzmann, G. Frenking, A. Stasch, *Chem. Commun.* **2012**, *48*, 9855.

[33] P. Bag, A. Porzelt, P. J. Altmann, S. Inoue, *J. Am. Chem. Soc.* **2017**, *139*, 14384–14387.

[34] Z. Feng, Y. Fang, H. Ruan, Y. Zhao, G. Tan, X. Wang, *Angew. Chem. Int. Ed.* **2020**, *59*, 6769–6774; *Angew. Chem.* **2020**, *132*, 6835–6840.

[35] a) J. D. Masuda, W. W. Schoeller, B. Donnadieu, G. Bertrand, *Angew. Chem. Int. Ed.* **2007**, *46*, 7052–7055; *Angew. Chem.* **2007**, *119*, 7182–7185; b) J. D. Masuda, W. W. Schoeller, B. Donnadieu, G. Bertrand, *J. Am. Chem. Soc.* **2007**, *129*, 14180–14181.

[36] a) M. Arrowsmith, H. Braunschweig, M. A. Celik, T. Dellermann, R. D. Dewhurst, W. C. Ewing, K. Hammond, T. Kramer, I. Krummenacher, J. Mies, K. Radacki, J. K. Schuster, *Nat. Chem.* **2016**, *8*, 890–894; b) G. Wang, J. E. Walley, D. A. Dickie, S. Pan, G. Frenking, R. J. Gilliard, *J. Am. Chem. Soc.* **2020**, *142*, 4560–4564; c) D. K. Roy, T. Tröster, F. Fantuzzi, R. D. Dewhurst, C. Lenczyk, K. Radacki, C. Pranckevicius, B. Engels, H. Braunschweig, *Angew. Chem. Int. Ed.* **2021**, *60*, 3812–3819; *Angew. Chem.* **2021**, *133*, 3856–3863.

[37] a) R. Kinjo, B. Donnadieu, M. A. Celik, G. Frenking, G. Bertrand, *Science* **2011**, *333*, 610–613; b) M. Rang, F. Fantuzzi, M. Arrowsmith, I. Krummenacher, E. Beck, R. Witte, A. Matler, A. Rempel, T. Bischof, K. Radacki, B. Engels, H. Braunschweig, *Angew. Chem. Int. Ed.* **2021**, *60*, 2963–2968; *Angew. Chem.* **2021**, *133*, 3000–3005; c) S. Hagspiel, M. Arrowsmith, F. Fantuzzi, A. Vargas, A. Rempel, A. Hermann, T. Brückner, H. Braunschweig, *Angew. Chem. Int. Ed.* **2021**, 60, 6446–6450; *Angew. Chem.* **2021**, *133*, 6519–6524.

[38] C. A. Dyker, V. Lavallo, B. Donnadieu, G. Bertrand, *Angew. Chem. Int. Ed.* **2008**, *47*, 3206–3209; *Angew. Chem.* **2008**, *120*, 3250–3253.

[39] S. K. Mellerup, Y. Cui, F. Fantuzzi, P. Schmid, J. T. Goettel, G. Bélanger-Chabot, M. Arrowsmith, I. Krummenacher, Q. Ye, V. Engel, B. Engels, H. Braunschweig, *J. Am. Chem. Soc.* **2019**, *141*, 16954–16960.

[40] a) P. Jerabek, H. W. Roesky, G. Bertrand, G. Frenking, *J. Am. Chem. Soc.* **2014**, *136*, 17123–17135; b) R. Jazzar, M. Soleilhavoup, G. Bertrand, *Chem. Rev.* **2020**, *120*, 4141–4168.

[41] K. V. S. Ranganath, S. Onitsuka, A. K. Kumar, J. Inanaga, *Catal. Sci. Technol.* **2013**, *3*, 2161.

[42] a) G. H. Gunasekar, K. Park, V. Ganesan, K. Lee, N.-K. Kim, K.-D. Jung, S. Yoon, *Chem. Mater.* **2017**, *29*, 6740–6748; b) Y. Li, Y. Dong, J.-L. Kan, X. Wu, Y.-B. Dong, *Org. Lett.* **2020**, *22*, 7363–7368.

[43] a) F. Fantuzzi, M. A. C. Nascimento, *Chem. Eur. J.* **2015**, *21*, 7814–7819; b) F. Fantuzzi, C. B. Coutinho, R. R. Oliveira, M. A. C. Nascimento, *Inorg. Chem.* **2018**, *57*, 3931–3940.

[44] S. T. Hashimoto, R. Hoshino, T. Hatanaka, Y. Ohki, K. Tatsumi, *Organometallics* **2014**, *33*, 921–929.

[45] a) V. Lavallo, Y. Canac, C. Präsang, B. Donnadieu, G. Bertrand, *Angew. Chem. Int. Ed.* **2005**, *44*, 5705–5709; *Angew. Chem.* **2005**, *117*, 5851–5855; b) V. Lavallo, Y. Canac, A. DeHope, B. Donnadieu, G. Bertrand, *Angew. Chem. Int. Ed.* **2005**, *44*, 7236–7239; *Angew. Chem.* **2005**, *117*, 7402–7405; c) M. Melaimi, R. Jazzar, M. Soleilhavoup, G. Bertrand, *Angew. Chem. Int. Ed.* **2017**, *56*, 10046–10068; *Angew. Chem.* **2017**, *129*, 10180–10203.

[46] D. S. Weinberger, M. Melaimi, C. E. Moore, A. L. Rheingold, G. Frenking, P. Jerabek, G. Bertrand, *Angew. Chem. Int. Ed.* **2013**, *52*, 8964–8967; *Angew. Chem.* **2013**, *125*, 9134–9137.

[47] K. C. Mondal, P. P. Samuel, H. W. Roesky, E. Carl, R. Herbst-Irmer, D. Stalke, B. Schwederski, W. Kaim, L. Ungur, L. F. Chibotaru, M. Hermann, G. Frenking, *J. Am. Chem. Soc.* **2014**, *136*, 1770–1773.

[48] R. Rubbiani, I. Kitanovic, H. Alborzinia, S. Can, A. Kitanovic, L. A. Onambele, M. Stefanopoulou, Y. Geldmacher, W. S. Sheldrick, G. Wolber, A. Prokop, S. Wölfl, I. Ott, *J. Med. Chem.* **2010**, *53*, 8608–8618.

[49] T. W. Hudnall, J. P. Moerdyk, C. W. Bielawski, *Chem. Commun.* **2010**, *46*, 4288–4290.

[50] T. W. Hudnall, A. G. Tennyson, C. W. Bielawski, *Organometallics* **2010**, *29*, 4569–4578.

[51] A. J. Arduengo III, J. R. Goerlich, W. J. Marshall, *Liebigs Ann.* **1997**, *1997*, 365–374.

[52] J. Kobayashi, S.-Y. Nakafuji, A. Yatabe, T. Kawashima, *Chem. Commun.* **2008**, 6233.

[53] A. R. Chianese, A. Kovacevic, B. M. Zeglis, J. W. Faller, R. H. Crabtree, *Organometallics* **2004**, *23*, 2461–2468.

[54] K. E. Krahulic, G. D. Enright, M. Parvez, R. Roesler, *J. Am. Chem. Soc.* **2005**, *127*, 4142–4143.

[55] B. O. Roos in *Advances in Chemical Physics Ab Initio Methods in Quantum Chemistry Part 2, Vol. 69* (Ed.: K. P. Lawley), Wiley, **1987**, pp. 399–445.

[56] a) C. Angeli, R. Cimiraglia, J.-P. Malrieu, *Chem. Phys. Lett.* **2001**, *350*, 297–305; b) C. Angeli, R. Cimiraglia, S. Evangelisti, T. Leininger, J. P. Malrieu, *J. Chem. Phys.* **2001**, *114*, 10252–10264; c) C. Angeli, R. Cimiraglia, J.-P. Malrieu, *J. Chem. Phys.* **2002**, *117*, 9138–915.

[57] S. J. P. Perdew, K. Burke, M. Ernzerhof, *Phys. Rev. Lett.* **1996**, *77*, 3865–3868.

[58] S. Grimme, J. Antony, S. Ehrlich, H. Krieg, *J. Chem. Phys.* **2010**, *132*, 154104.

[59] S. Grimme, S. Ehrlich, L. Goerigk, *J. Comput. Chem.* **2011**, *32*, 1456–1465.

[60] F. Weigend, R. Ahlrichs, *Phys. Chem. Chem. Phys.* **2005**, *7*, 3297.

[61] G. Knizia, *J. Chem. Theory Comput.* **2013**, *9*, 4834–4843.

[62] F. Weinhold, C. Landis, E. Glendening, *Int. Rev. Phys. Chem.* **2016**, *35*, 399–440.

[63] a) E. D. Glendening, F. Weinhold, *J. Comput. Chem.* **1998**, *19*, 593–609; b) E. D. Glendening, F. Weinhold, *J. Comput. Chem.* **1998**, *19*, 610–627; c) E. D. Glendening, J. K. Badenhoop, F. Weinhold, *J. Comput. Chem.* **1998**, *19*, 628–646.

[64] F. W. Bobrowicz, W. A. Goddard III in *Methods of Electronic Structure Theory* (Ed.: H. F. Schaefer), *Springer*, **1977**, p. 79–127.

[65] a) I. Mayer, *Chem. Phys. Lett.* **1983**, *97*, 270–274; b) I. Mayer, *Int. J. Quantum Chem.* **1984**, *26*, 151–154.

[66] M. J. Frisch, G. W. Trucks, H. B. Schlegel, G. E. Scuseria, M. A. Robb, J. R. Cheeseman, G. Scalmani, V. Barone, B. Mennucci, G. A. Petersson, H. Nakatsuji, M. Caricato, X. Li, H. P. Hratchian, A. F. Izmaylov, J. Bloino, G. Zheng, J. L. Sonnenberg, M. Hada, M. Ehara, K. Toyota, R. Fukuda, J. Hasegawa, M. Ishida, T. Nakajima, Y. Honda, O. Kitao, H. Nakai, T. Vreven, J. A. Montgomery Jr., J. E. Peralta, F. Ogliaro, M. Bearpark, J. J. Heyd, E. Brothers, K. N. Kudin, V. N. Staroverov, R. Kobayashi, J. Normand, K. Raghavachari, A. Rendell, J. C. Burant, S. S. Iyengar, J. Tomasi, M. Cossi, N. Rega, J. M. Millam, M. Klene, J. E. Knox, J. B. Cross, V. Bakken, C. Adamo, J. Jaramillo, R. Gomperts, R. E. Stratmann, O. Yazyev, A. J. Austin, R. Cammi, C. Pomelli, J. W. Ochterski, R. L. Martin, K. Morokuma, V. G. Zakrzewski, G. A. Voth, P. Salvador, J. J. Dannenberg, S. Dapprich, A. D. Daniels, Ö. Farkas, J. B. Foresman, J. V Ortiz, J. Cioslowski, D. J. Fox, *Gaussian 16, Revision B.01*, Gaussian, Inc., Wallingford CT, **2016**.

[67] G. Kresse, J. Furthmüller, *Phys. Rev. B* **1996**, *54*, 11169–11186.

[68] S a) F. Neese, *WIREs Comput. Mol. Sci.* **2012**, *2*, 73–78; b) F. Neese, F. Wennmohs, U. Becker, C. Riplinger, *J. Chem. Phys.* **2020**, *152*, 224108.

[69] T. Lu, F. Chen, *J. Comput. Chem.* **2012**, *33*, 580–592.

[70] E. D. Glendening, C. R. Landis, F. Weinhold, *J. Comput. Chem.* **2019**, jcc.25873.

[71] J. Li, R. McWeeny, *Int. J. Quantum Chem.* **2002**, *89*, 208–216.

[72] a) K. Yamaguchi, *Chem. Phys. Lett.* **1975**, *33*, 330–335; b) S. Yamanaka, M. Okumura, M. Nakano, K. Yamaguchi, *J. Mol. Struct.* **1994**, *310*, 205–218; c) M. Nakano, *Top. Curr. Chem.* **2017**, *375*, 47.